Analysis and Implementation of a Novel Bidirectional DC–DC Converter

Lung-Sheng Yang and Tsorng-Juu Liang, *Senior Member, IEEE*

***Abstract*—A novel bidirectional dc–dc converter is presented in this paper. The circuit configuration of the proposed converter is very simple. The proposed converter employs a coupled inductor with same winding turns in the primary and secondary sides. In step-up mode, the primary and secondary windings of the coupled inductor are operated in parallel charge and series discharge to achieve high step-up voltage gain. In step-down mode, the primary and secondary windings of the coupled inductor are operated in series charge and parallel discharge to achieve high step-down voltage gain. Thus, the proposed converter has higher step-up and step-down voltage gains than the conventional bidirectional dc–dc boost/buck converter. Under same electric specifications for the proposed converter and the conventional bidirectional boost/buck converter, the average value of the switch current in the proposed converter is less than the conventional bidirectional boost/buck converter. The operating principle and steady-state analysis are discussed in detail. Finally, a 14/42-V prototype circuit is implemented to verify the performance for the automobile dual-battery system.**

***Index Terms*—Bidirectional dc–dc converter, coupled inductor.**

I. Introduction

BIDIRECTIONAL dc–dc converters are used to transfer the power between two dc sources in either direction. These converters are widely used in applications, such as hybrid electric vehicle energy systems [1]–[4], uninterrupted power supplies [5], [6], fuel-cell hybrid power systems [7]–[10], photovoltaic hybrid power systems [11], [12], and battery chargers [13]–[15]. Many bidirectional dc–dc converters have been researched. The bidirectional dc–dc flyback converters are more attractive due to simple structure and easy control [2], [16], [17]. However, these converters suffer from high voltage stresses on the power devices due to the leakage inductor energy of the transformer. In order to recycle the leakage inductor energy and to minimize the voltage stress on the power devices, some literatures present the energy regeneration techniques to clamp the voltage stress on the power devices and to recycle the leakage inductor energy [18], [19]. Some literatures research the isolated bidirectional dc–dc converters, which include the half-bridge [8], [9], [20], [21] and full-bridge types [13], [22]. These converters can provide high step-up and step-down voltage gain by adjusting the turns ratio of the transformer. For non-isolated applications, the non-isolated bidirectional dc–dc converters, which include the conventional boost/buck [1], [5], [12], [14], multilevel [4], three-level [10], sepic/zeta [23], switched capacitor [24], and coupled inductor types [25], are presented. The multilevel type is a magneticless converter, but 12 switches are used in this converter. If higher step-up and step-down voltage gains are required, more switches are needed. This control circuit becomes more complicated. In the three-level type, the voltage stress across the switches on the three-level type is only half of the conventional type. However, the step-up and step-down voltage gains are low. Since the sepic/zeta type is combined of two power stages, the conversion efficiency will be decreased. The switched capacitor and coupled inductor types can provide high step-up and step-down voltage gains. However, their circuit configurations are complicated. Fig. 1 shows the conventional bidirectional dc–dc boost/buck converter which is simple structure and easy control. However, the step-up and step-down voltage gains are low.

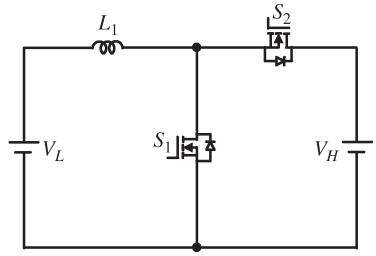

Fig. 1. Conventional bidirectional dc–dc boost/buck converter.

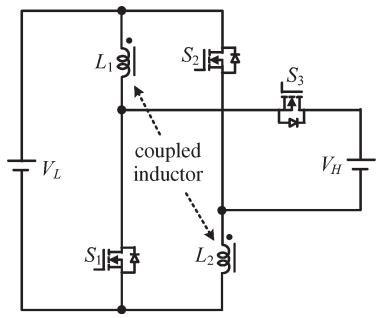

Fig. 2. Proposed bidirectional dc–dc converter.

A modified dc–dc boost converter is presented [26]. The voltage gain of this converter is higher than the conventional dc–dc boost converter. Based on this converter, a novel bidirectional dc–dc converter is proposed, as shown in Fig. 2. The proposed converter employs a coupled inductor with same

Manuscript received August 4, 2010; revised December 8, 2010 and February 23, 2011; accepted March 14, 2011. Date of publication April 5, 2011; date of current version October 4, 2011.

L.-S. Yang is with the Department of Electrical Engineering, Far East University, Tainan 744, Taiwan (e-mail: yanglusheng@yahoo.com.tw).

T.-J. Liang is with the Department of Electrical Engineering, National Cheng Kung University, Tainan 701, Taiwan (e-mail: tgliang@mail.ncku.edu.tw).

Digital Object Identifier 10.1109/TIE.2011.2134060

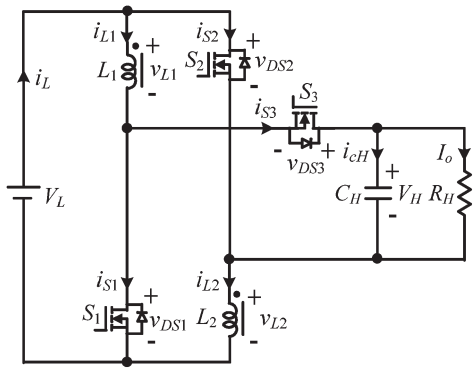

Fig. 3. Proposed converter in step-up mode.

winding turns in the primary and secondary sides. Comparing to the proposed converter and the conventional bidirectional boost/buck converter, the proposed converter has the following advantages: 1) Higher step-up and step-down voltage gains and 2) lower average value of the switch current under same electric specifications. The following sections will describe the operating principles and steady-state analysis for the step-up and step-down modes. In order to analyze the steady-state characteristics of the proposed converter, some conditions are assumed: The ON-state resistance $R_{DS(ON)}$ of the switches and the equivalent series resistances of the coupled inductor and capacitors are ignored; the capacitor is sufficiently large; and the voltages across the capacitor can be treated as constant.

II. Step-Up Mode

The proposed converter in step-up mode is shown in Fig. 3. The pulsewidth modulation (PWM) technique is used to control the switches S_1 and S_2 simultaneously. The switch S_3 is the synchronous rectifier.

Since the primary and secondary winding turns of the coupled inductor is same, the inductance of the coupled inductor in the primary and secondary sides are expressed as

$$L_1 = L_2 = L. \tag{1}$$

Thus, the mutual inductance M of the coupled inductor is given by

$$M = k\sqrt{L_1 L_2} = kL \tag{2}$$

where k is the coupling coefficient of the coupled inductor. The voltages across the primary and secondary windings of the coupled inductor are as follows:

$$v_{L1} = L_1\frac{di_{L1}}{dt} + M\frac{di_{L2}}{dt} = L\frac{di_{L1}}{dt} + kL\frac{di_{L2}}{dt} \tag{3}$$

$$v_{L2} = M\frac{di_{L1}}{dt} + L_2\frac{di_{L2}}{dt} = kL\frac{di_{L1}}{dt} + L\frac{di_{L2}}{dt}. \tag{4}$$

Fig. 4 shows some typical waveforms in continuous conduction mode (CCM) and discontinuous conduction mode (DCM). The operating principles and steady-state analysis of CCM and DCM are described as follows.

A. CCM Operation

1) Mode 1: During this time interval $[t_0, t_1]$, S_1 and S_2 are turned on and S_3 is turned off. The current flow path is shown in Fig. 5(a). The energy of the low-voltage side V_L is transferred to the coupled inductor. Meanwhile, the primary and secondary windings of the coupled inductor are in parallel. The energy stored in the capacitor C_H is discharged to the load. Thus, the voltages across L_1 and L_2 are obtained as

$$v_{L1} = v_{L2} = V_L. \tag{5}$$

Substituting (3) and (4) into (5), yielding

$$\frac{di_{L1}(t)}{dt} = \frac{di_{L2}(t)}{dt} = \frac{V_L}{(1+k)L}, \quad t_0 \le t \le t_1. \tag{6}$$

2) Mode 2: During this time interval $[t_1, t_2]$, S_1 and S_2 are turned off and S_3 is turned on. The current flow path is shown in Fig. 5(b). The low-voltage side V_L and the coupled inductor are in series to transfer their energies to the capacitor C_H and the load. Meanwhile, the primary and secondary windings of the coupled inductor are in series. Thus, the following equations are found to be

$$i_{L1} = i_{L2} \tag{7}$$

$$v_{L1} + v_{L2} = V_L - V_H. \tag{8}$$

Substituting (3), (4), and (7) into (8), yielding

$$\frac{di_{L1}(t)}{dt} = \frac{di_{L2}(t)}{dt} = \frac{V_L - V_H}{2(1+k)L}, \quad t_1 \le t \le t_2. \tag{9}$$

By using the state-space averaging method, the following equation is derived from (6) and (9):

$$\frac{DV_L}{(1+k)L} + \frac{(1-D)(V_L - V_H)}{2(1+k)L} = 0. \tag{10}$$

Simplifying (10), the voltage gain is given as

$$G_{CCM(step-up)} = \frac{V_H}{V_L} = \frac{1+D}{1-D}. \tag{11}$$

B. DCM Operation

1) Mode 1: During this time interval $[t_0, t_1]$, S_1 and S_2 are turned on and S_3 is turned off. The current flow path is shown in Fig. 5(a). The operating principle is same as that for the mode 1 of CCM operation. From (6), the two peak currents through the primary and secondary windings of the coupled inductor are given by

$$I_{L1p} = I_{L2p} = \frac{V_L D T_s}{(1+k)L}. \tag{12}$$

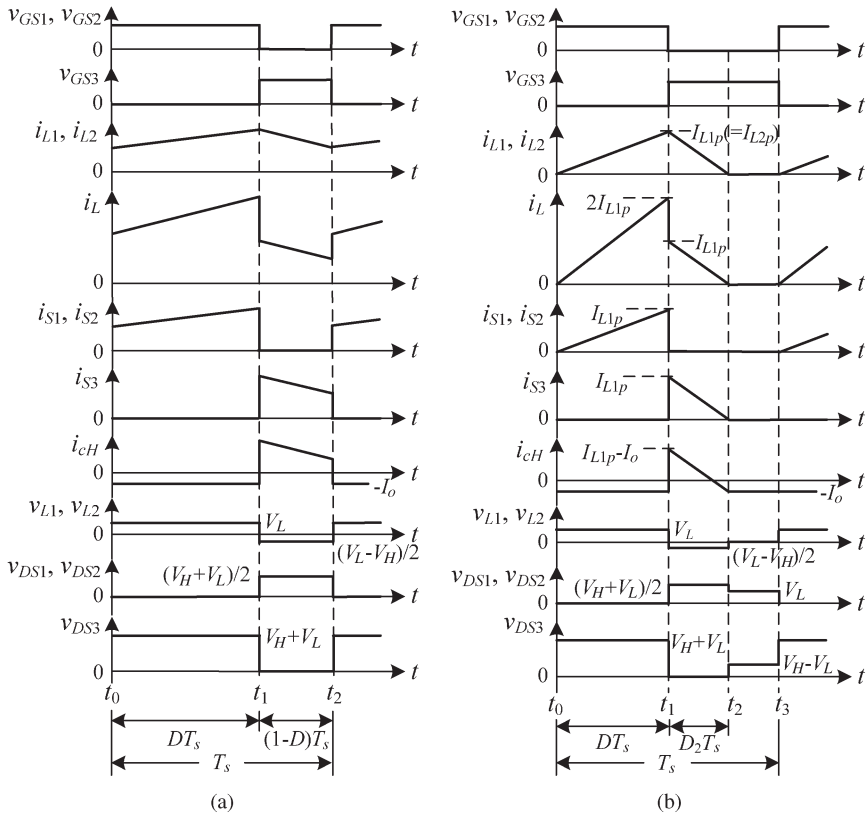

Fig. 4. Some typical waveforms of the proposed converter in step-up mode. (a) CCM operation. (b) DCM operation.

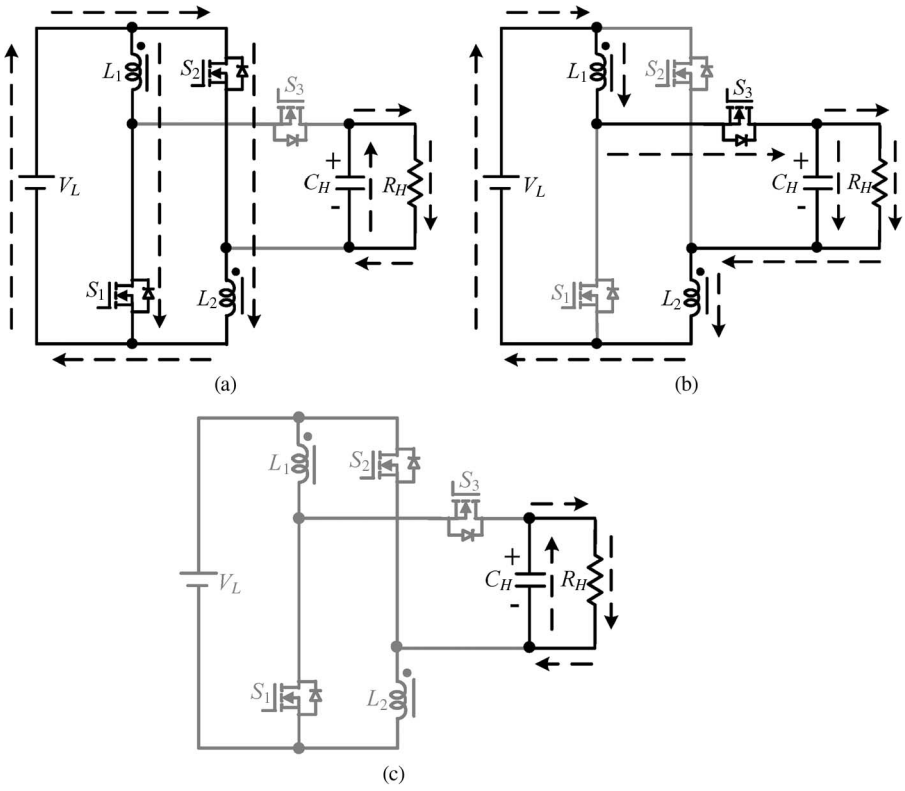

Fig. 5. Current flow path of the proposed converter in step-up mode. (a) Mode 1. (b) Mode 2. (c) Mode 3 for DCM operation.

2) Mode 2: During this time interval $[t_1, t_2]$, S_1 and S_2 are turned off and S_3 is turned on. The current flow path is shown in Fig. 5(b). The low-voltage side V_L and the coupled inductor are in series to transfer their energies to the capacitor C_H and the load. Meanwhile, the primary and secondary windings of the coupled inductor are in series. The currents i_{L1} and i_{L2} through

the primary and secondary windings of the coupled inductor are decreased to zero at $t = t_2$. From (9), another expression of I_{L1p} and I_{L2p} is given by

$$I_{L1p} = I_{L2p} = \frac{(V_H - V_L)D_2T_s}{2(1+k)L}. \tag{13}$$

3) Mode 3: During this time interval $[t_2, t_3]$, S_1 and S_2 are still turned off and S_3 is still turned on. The current flow path is shown in Fig. 5(c). The energy stored in the coupled inductor is zero. Thus, i_{L1} and i_{L2} are equal to zero. The energy stored in the capacitor C_H is discharged to the load.

From (12) and (13), D_2 is derived as follows:

$$D_2 = \frac{2DV_L}{V_H - V_L}. \tag{14}$$

From Fig. 4(b), the average value of the output capacitor current during each switching period is given by

$$I_{cH} = \frac{\frac{1}{2}D_2T_sI_{L1p} - I_oT_s}{T_s} = \frac{1}{2}D_2I_{L1p} - I_o. \tag{15}$$

Substituting (12) and (14) into (15), I_{cH} is derived as

$$I_{cH} = \frac{D^2V_L^2T_s}{(1+k)L(V_H - V_L)} - \frac{V_H}{R_H}. \tag{16}$$

Since I_{cH} is equal to zero under steady state, (16) can be rewritten as follows:

$$\frac{D^2V_L^2T_s}{(1+k)L(V_H - V_L)} = \frac{V_H}{R_H}. \tag{17}$$

Then, the normalized inductor time constant is defined as

$$\tau_{LH} \equiv \frac{L}{R_HT_s} = \frac{Lf_s}{R_H} \tag{18}$$

where f_s is the switching frequency.

Substituting (18) into (17), the voltage gain is given by

$$G_{DCM(step-up)} = \frac{V_H}{V_L} = \frac{1}{2} + \sqrt{\frac{1}{4} + \frac{D^2}{(1+k)\tau_{LH}}}. \tag{19}$$

C. Boundary Operating Condition of CCM and DCM

When the proposed converter in step-up mode is operated in boundary conduction mode (BCM), the voltage gain of CCM operation is equal to the voltage gain of DCM operation. From (11) and (19), the boundary normalized inductor time constant $\tau_{LH,B}$ can be derived as follows:

$$\tau_{LH,B} = \frac{D(1-D)^2}{2(1+k)(1+D)}. \tag{20}$$

The curve of $\tau_{LH,B}$ is plotted in Fig. 6. If τ_{LH} is larger than $\tau_{LH,B}$, the proposed converter in step-up mode is operated in CCM.

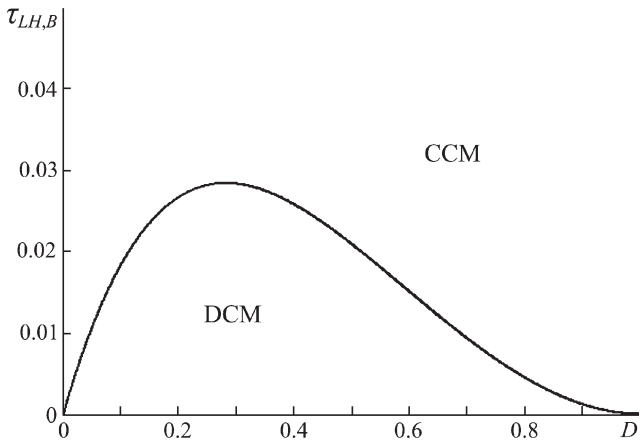

Fig. 6. Boundary condition of the proposed converter in step-up mode (assuming $k = 1$).

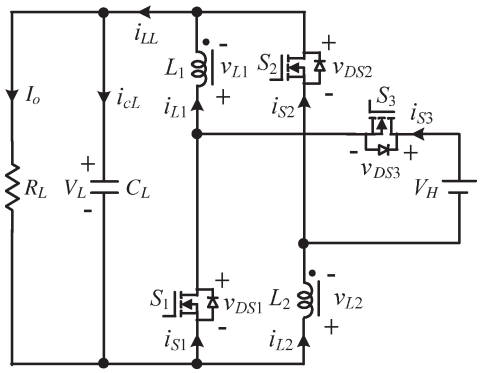

Fig. 7. Proposed converter in step-down mode.

III. Step-Down Mode

Fig. 7 shows the proposed converter in step-down mode. The PWM technique is used to control the switch S_3. The switches S_1 and S_2 are the synchronous rectifiers. Fig. 8 shows some typical waveforms in CCM and DCM. The operating principle and steady-state analysis of CCM and DCM are described as follows.

A. CCM Operation

1) Mode 1: During this time interval $[t_0, t_1]$, S_3 is turned on and S_1/S_2 are turned off. The current flow path is shown in Fig. 9(a). The energy of the high-voltage side V_H is transferred to the coupled inductor, the capacitor C_L, and the load. Meanwhile, the primary and secondary windings of the coupled inductor are in series. Thus, the following equations are given as:

$$i_{L1} = i_{L2} \tag{21}$$

$$v_{L1} + v_{L2} = V_H - V_L. \tag{22}$$

Substituting (3), (4), and (21) into (22), yielding

$$\frac{di_{L1}(t)}{dt} = \frac{di_{L2}(t)}{dt} = \frac{V_H - V_L}{2(1+k)L}, \quad t_0 \le t \le t_1. \tag{23}$$

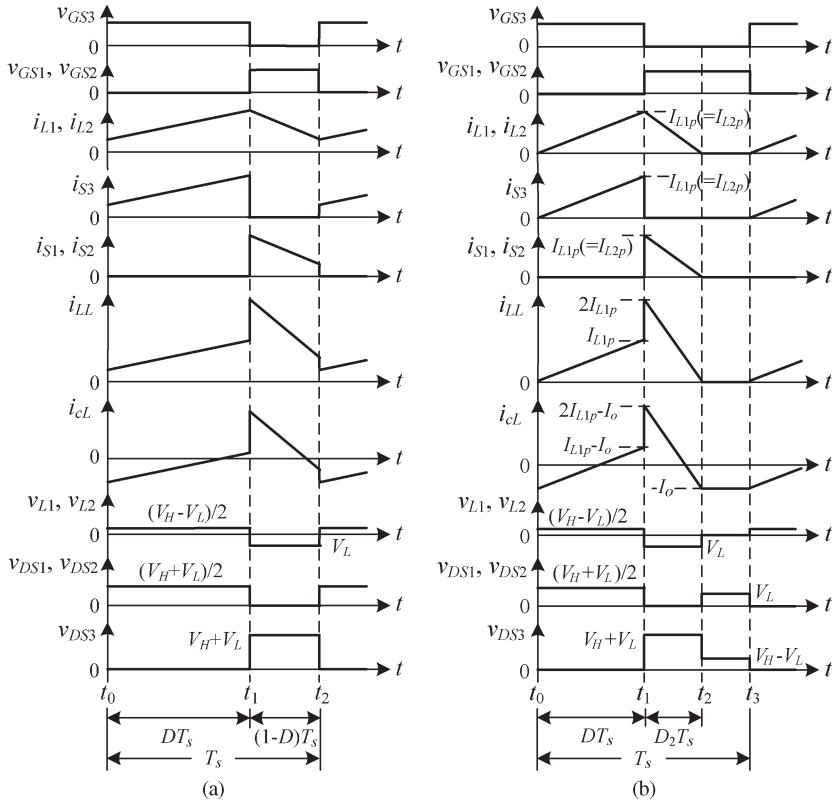

Fig. 8. Some typical waveforms of the proposed converter in step-down mode. (a) CCM operation. (b) DCM operation.

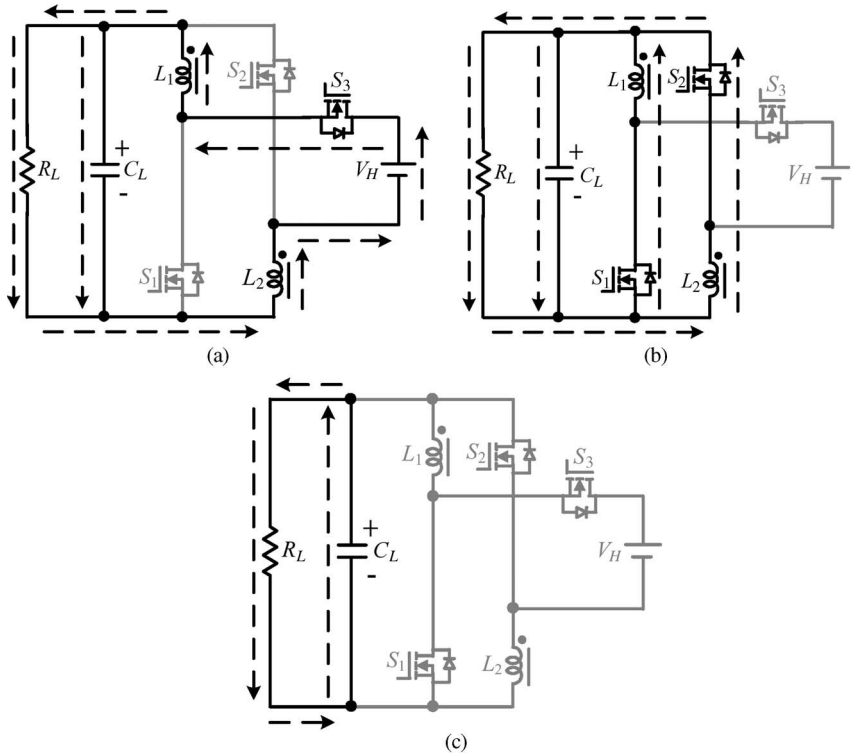

Fig. 9. Current flow path of the proposed converter in step-down mode. (a) Mode 1. (b) Mode 2. (c) Mode 3 for DCM operation.

2) Mode 2: During this time interval $[t_1, t_2]$, S_3 is turned off and S_1/S_2 are turned on. The current flow path is shown in Fig. 9(b). The energy stored in the coupled inductor is released to the capacitor C_L and the load. Meanwhile, the primary and secondary windings of the coupled inductor are in parallel. Thus, the voltages across L_1 and L_2 are derived as

$$v_{L1} = v_{L2} = -V_L. \tag{24}$$

Substituting (3) and (4) into (24), yielding

$$\frac{di_{L1}(t)}{dt} = \frac{di_{L2}(t)}{dt} = -\frac{V_L}{(1+k)L}, \quad t_1 \le t \le t_2. \tag{25}$$

By using the state space averaging method, the following equation is obtained from (23) and (25):

$$\frac{D(V_H - V_L)}{2(1+k)L} - \frac{(1-D)V_L}{(1+k)L} = 0. \tag{26}$$

Simplifying (26), the voltage gain is found to be

$$G_{CCM(step-down)} = \frac{V_L}{V_H} = \frac{D}{2-D}. \tag{27}$$

B. DCM Operation

The operating modes can be divided into three modes, defined as modes 1, 2, and 3.

1) Mode 1: During this time interval $[t_0, t_1]$, S_3 is turned on and S_1/S_2 are turned off. The current flow path is shown in Fig. 9(a). The operating principle is same as that for the mode 1 of CCM operation. From (23), the two peak currents through the primary and secondary windings of the coupled inductor are given by

$$I_{L1p} = I_{L2p} = \frac{(V_H - V_L)DT_s}{2(1+k)L}. \tag{28}$$

2) Mode 2: During this time interval $[t_1, t_2]$, S_3 is turned off and S_1/S_2 are turned on. The current flow path is shown in Fig. 9(b). The energy stored in the coupled inductor is released to the capacitor C_L and the load. Meanwhile, the primary and secondary windings of the coupled inductor are in parallel. The currents i_{L1} and i_{L2} through the primary and secondary windings of the coupled inductor are decreased to zero at $t = t_2$. From (25), another expression of I_{L1p} and I_{L2p} is given as

$$I_{L1p} = I_{L2p} = \frac{V_L D_2 T_s}{(1+k)L}. \tag{29}$$

3) Mode 3: During this time interval $[t_2, t_3]$, S_3 is still turned off and S_1/S_2 are still turned on. The current flow path is shown in Fig. 9(c). The energy stored in the coupled inductor is zero. Thus, i_{L1} and i_{L2} are equal to zero. The energy stored in the capacitor C_L is discharged to the load.

From (28) and (29), D_2 is derived as follows:

$$D_2 = \frac{D(V_H - V_L)}{2V_L}. \tag{30}$$

From Fig. 9(b), the average value of the output capacitor current during each switching period is given by

$$\begin{aligned} I_{cL} &= \frac{\frac{1}{2}DT_s I_{L1p} + \frac{1}{2}D_2 T_s (2I_{L1p}) - I_o T_s}{T_s} \\ &= \frac{1}{2}DI_{L1p} + D_2 I_{L1p} - I_o. \end{aligned} \tag{31}$$

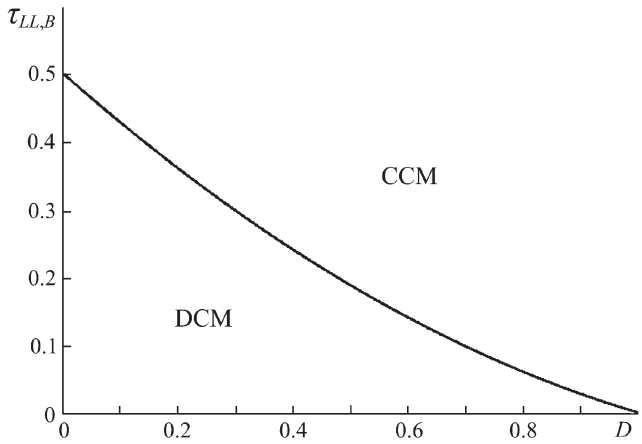

Fig. 10. Boundary condition of the proposed converter in step-down mode (assuming $k = 1$).

Substituting (28) and (30) into (31), I_{cL} is derived as

$$I_{cL} = \frac{D^2 T_s \left[(V_H - V_L)V_L + (V_H - V_L)^2\right]}{4(1+k)LV_L} - \frac{V_L}{R_L}. \tag{32}$$

Since I_{cL} is equal to zero under steady state, (32) can be rewritten as follows:

$$\frac{D^2 T_s \left[(V_H - V_L)V_L + (V_H - V_L)^2\right]}{4(1+k)LV_L} = \frac{V_L}{R_L}. \tag{33}$$

Then, the normalized inductor time constant is defined as

$$\tau_{LL} \equiv \frac{L}{R_L T_s} = \frac{Lf_s}{R_L}. \tag{34}$$

Substituting (34) into (33), the voltage gain of DCM operation is given by

$$G_{DCM(step-down)} = \frac{V_L}{V_H} = \frac{2}{1 + \sqrt{1 + \frac{16(1+k)\tau_{LL}}{D^2}}}. \tag{35}$$

C. Boundary Operating Condition of CCM and DCM

When the proposed converter in step-down mode is operated in BCM, the voltage gain of CCM operation is equal to the voltage gain of DCM operation. From (27) and (35), the boundary normalized inductor time constant $\tau_{LL,B}$ can be derived as follows:

$$\tau_{LL,B} = \frac{(1-D)(2-D)}{2(1+k)}. \tag{36}$$

The curve of $\tau_{LL,B}$ is plotted in Fig. 10. If τ_{LL} is larger than $\tau_{LL,B}$, the proposed converter in the step-down mode is operated in CCM.

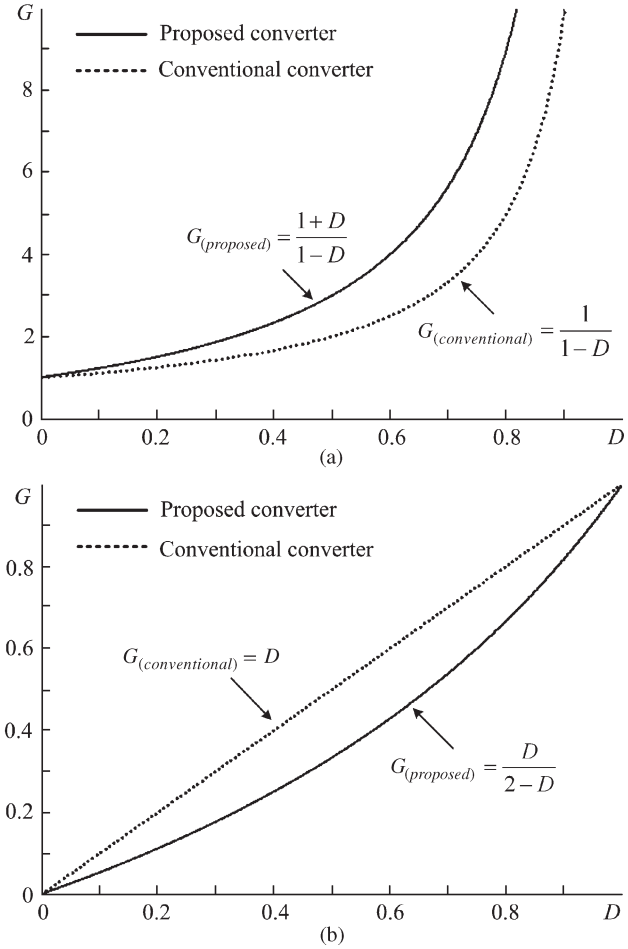

Fig. 11. Voltage gain of the proposed converter and conventional bidirectional boost/buck converter in CCM operation. (a) Step-up mode. (b) Step-down mode.

IV. Comparison of the Proposed Converter and Conventional Bidirectional Boost/Buck Converter

A. Voltage Gain

The curves of the voltage gain of the proposed converter and conventional bidirectional boost/buck converter in CCM operation are plotted in Fig. 11. It is seen that the step-up and step-down voltage gains of the proposed converter are higher than the conventional bidirectional boost/buck converter.

B. Voltage Stress on the Switches

From Figs. 4(a) and 8(a), the voltage stresses on S_1, S_2, and S_3 in the proposed converter are derived as

$$\begin{cases} V_{DS1} = V_{DS2} = \frac{V_H + V_L}{2} \\ V_{DS3} = V_H + V_L. \end{cases} \tag{37}$$

As to the voltage stresses on S_1 and S_2 in the conventional bidirectional boost/buck converter are given as

$$V_{DS1} = V_{DS2} = V_H. \tag{38}$$

Therefore, if the proposed converter is used for high step-up/down voltage-gain application, the rated voltage of S_1 and S_2 in the proposed converter can be selected to be lower than the conventional converter. Also, the rated voltage of S_3 in the proposed converter can be selected as same as the conventional converter.

C. Average Value of the Switch-Current

When the proposed converter in step-up mode is operated in CCM, the average value of the input current i_L is found from Fig. 4(a)

$$\begin{aligned} I_{L(proposed)} &= \frac{2I_{L1(proposed)}DT_s + I_{L1(proposed)}(1-D)T_s}{T_s} \\ &= (1+D)I_{L1(proposed)} \end{aligned} \tag{39}$$

where I_{L1} is the average value of i_{L1}. When the conventional bidirectional boost/buck converter in step-up mode is also operated in CCM, the average value of the input current i_L is given by

$$I_{L(conventional)} = I_{L1(conventional)}. \tag{40}$$

Under same electric specifications for the proposed converter and conventional bidirectional boost/buck converter, the input power can be expressed as

$$P_{in} = V_L I_{L(conventional)} = V_L I_{L(proposed)}. \tag{41}$$

Substituting (39) and (40) into (41), yielding

$$I_{L1(proposed)} = \frac{I_{L1(conventional)}}{1+D}. \tag{42}$$

When the proposed converter in step-down mode is operated in CCM, the average value of the current i_{LL} is found from Fig. 8(a)

$$\begin{aligned} I_{LL(proposed)} &= \frac{I_{L1(proposed)}DT_s + 2I_{L1(proposed)}(1-D)T_s}{T_s} \\ &= (2-D)I_{L1(proposed)}. \end{aligned} \tag{43}$$

Under same electric specifications for the proposed converter and conventional bidirectional boost/buck converter, the output power can be obtained as

$$P_o = V_L I_{L1(conventional)} = V_L I_{LL(proposed)}. \tag{44}$$

From (43) and (44), the following equation is derived as:

$$I_{L1(proposed)} = \frac{I_{L1(conventional)}}{2-D}. \tag{45}$$

From (42) and (45), one can know that the average value of the switch current in the proposed converter is less than the conventional bidirectional boost/buck converter.

D. Efficiency Analysis

For the proposed converter, the equivalent circuits in step-up mode are shown in Fig. 12. r_{L1} and r_{L2} represent the equivalent series resistor (ESR) of the primary and secondary windings of the coupled inductor. r_{S1}, r_{S2}, and r_{S3} denote the ON-state resistance of S_1, S_2, and S_3, respectively. When S_1/S_2 are

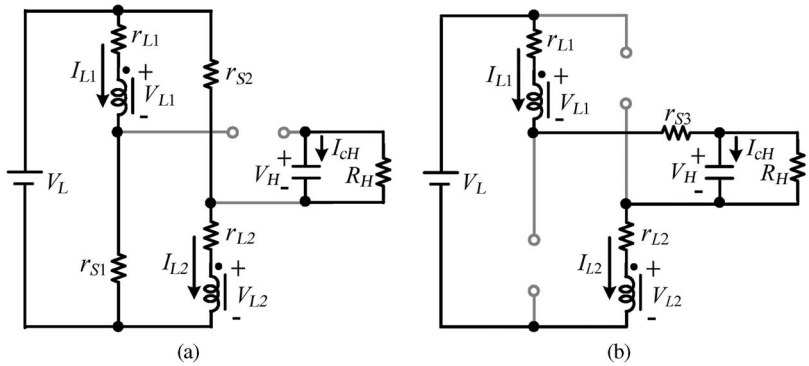

Fig. 12. Equivalent circuit of the proposed converter in step-up mode. (a) S_1/S_2 ON and S_3 OFF. (b) S_1/S_2 OFF and S_3 ON.

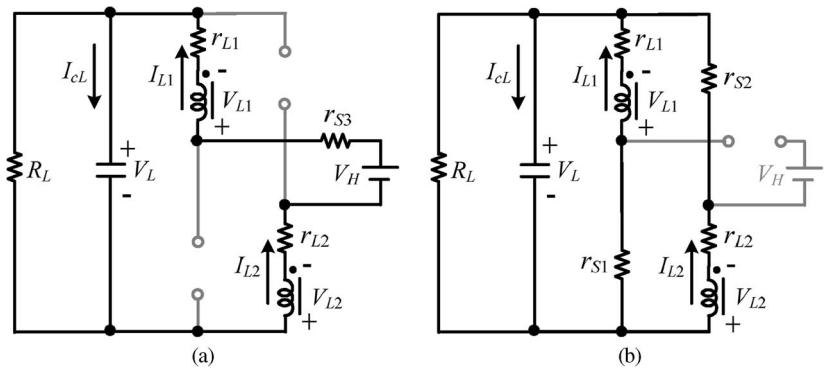

Fig. 13. Equivalent circuit of the proposed converter in step-down mode. (a) S_1/S_2 ON and S_3 OFF. (b) S_1/S_2 OFF and S_3 ON.

turned on and S_3 is turned off, the equivalent circuit is shown in Fig. 12(a). The average values of i_{cH} and v_{L1} are obtained as

$$I_{cH}^{I} = -\frac{V_H}{R_H} \tag{46}$$

$$V_{L1}^{I} = V_L - I_{L1}(r_{L1} + r_{S1}). \tag{47}$$

When S_1/S_2 are turned off and S_3 is turned on, the equivalent circuit is shown in Fig. 12(b). The average values of i_{cH} and v_{L1} are derived as

$$I_{cH}^{II} = I_{L1} - \frac{V_H}{R_H} \tag{48}$$

$$V_{L1}^{II} = \frac{V_L - V_H - I_{L1}(r_{L1} + r_{S3} + r_{L2})}{2}. \tag{49}$$

By using the ampere-second balance principle on C_H, the following equations are obtained as:

$$\int_0^{DT_s} I_{cH}^{I} dt + \int_0^{(1-D)T_s} I_{cH}^{II} dt = 0. \tag{50}$$

Substituting (46) and (48) into (50), I_{L1} is given by

$$I_{L1} = \frac{V_H}{(1-D)R_H}. \tag{51}$$

Using the volt-second balance principle on L_1 yields

$$\int_0^{DT_s} V_{L1}^{I} dt + \int_0^{(1-D)T_s} V_{L1}^{II} dt = 0. \tag{52}$$

Substituting (47) and (49) into (52), the actual voltage gain is derived as

$$\frac{V_H}{V_L} = \frac{1+D}{1-D} \cdot \frac{(1-D)^2 R_H}{(1-D)^2 R_H + 2D(r_{L1} + r_{S1}) + (1-D)(r_{L1} + r_{S3} + r_{L2})}. \tag{53}$$

The input power and output power are obtained as

$$P_{in} = 2V_L I_{L1} D + V_L I_{L1}(1-D) = \frac{(1+D)V_L V_H}{(1-D)R_H} \tag{54}$$

$$P_o = \frac{V_H^2}{R_H}. \tag{55}$$

From (53)–(55), the efficiency is found to be

$$\eta = \frac{P_o}{P_{in}} = \frac{(1-D)^2 R_H}{(1-D)^2 R_H + 2D(r_{L1} + r_{S1}) + (1-D)(r_{L1} + r_{S3} + r_{L2})}. \tag{56}$$

For the proposed converter, the equivalent circuits in step-down mode are shown in Fig. 13. When S_3 is turned on and S_1/S_2 are turned off, the equivalent circuit is shown in Fig. 13(a). The average values of i_{cL} and v_{L1} are obtained as

$$I_{cL}^{I} = I_{L1} - \frac{V_L}{R_L} \tag{57}$$

$$V_{L1}^{I} = \frac{V_H - V_L - I_{L1}(r_{S3} + r_{L1} + r_{L2})}{2}. \tag{58}$$

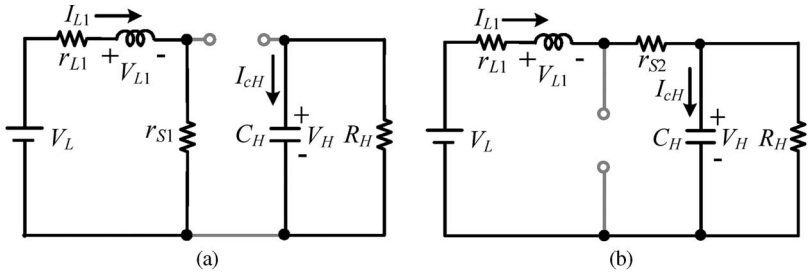

Fig. 14. Equivalent circuit of the conventional converter in step-up mode. (a) S_1 ON and S_2 OFF. (b) S_1 OFF and S_2 ON.

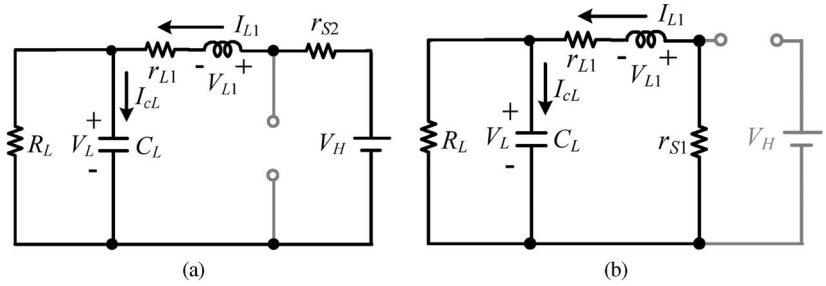

Fig. 15. Equivalent circuit of the conventional converter in step-down mode. (a) S_2 ON and S_1 OFF. (b) S_2 OFF and S_1 ON.

When S_3 is turned off and S_1/S_2 are turned on, the equivalent circuit is shown in Fig. 13(b). The average values of i_{cL} and v_{L1} are derived as

$$I_{cL}^{II} = 2I_{L1} - \frac{V_L}{R_L} \tag{59}$$

$$V_{L1}^{II} = -V_{\rm L} - I_{L1}(r_{L1} + r_{S1}). \tag{60}$$

By using the ampere-second balance principle on C_L, the following equations are obtained as:

$$\int_0^{DT_s} I_{cL}^{I} dt + \int_0^{(1-D)T_s} I_{cL}^{II} dt = 0. \tag{61}$$

Substituting (57) and (59) into (61), I_{L1} is obtained as

$$I_{L1} = \frac{V_L}{(2-D)R_L}. \tag{62}$$

Using the volt-second balance principle on L_1 yields

$$\int_0^{DT_s} V_{L1}^{I} dt + \int_0^{(1-D)T_s} V_{L1}^{II} dt = 0. \tag{63}$$

Substituting (58) and (60) into (63), the actual voltage gain is derived as

$$\frac{V_L}{V_H} = \frac{D}{2-D} \cdot \frac{(2-D)^2 R_L}{(2-D)^2 R_L + D(r_{S3} + r_{L1} + r_{L2}) + 2(1-D)(r_{L1} + r_{S1})}. \tag{64}$$

The input power and output power are obtained as

$$P_{in} = V_H I_{L1} D = \frac{D V_L V_H}{(2-D)R_L} \tag{65}$$

$$P_o = \frac{V_L^2}{R_L}. \tag{66}$$

From (64)–(66), the efficiency is found to be

$$\eta = \frac{P_o}{P_{in}} = \frac{(2-D)^2 R_L}{(2-D)^2 R_L + D(r_{S3} + r_{L1} + r_{L2}) + 2(1-D)(r_{L1} + r_{S1})}. \tag{67}$$

For the conventional converter, the equivalent circuits in step-up mode are shown in Fig. 14. r_{L1} represents the ESR of the inductor. r_{S1} and r_{S2} denote ON-state resistance of S_1 and S_2. According to the foregoing method, the efficiency is derived as follows:

$$\eta = \frac{P_o}{P_{in}} = \frac{(1-D)^2 R_H}{(1-D)^2 R_H + D(r_{L1} + r_{S1}) + (1-D)(r_{L1} + r_{S2})}. \tag{68}$$

For the conventional converter, the equivalent circuits in step-down mode are shown in Fig. 15. According to the foregoing method, the efficiency is derived as follows:

$$\eta = \frac{P_o}{P_{in}} = \frac{R_L}{R_L + D(r_{S2} + r_{L1}) + (1-D)(r_{L1} + r_{S1})}. \tag{69}$$

In order to compare the calculated efficiency for the proposed converter and the conventional converter, some parameters of three cases are assumed as follows:

1) Case 1: $r_{L1} = r_{L2} = 11$ mΩ, $r_{S1} = r_{S2} = r_{S3} = 23$ mΩ, $V_H = 42$ V, and $V_L = 21$ V.
2) Case 2: $r_{L1} = r_{L2} = 11$ mΩ, $r_{S1} = r_{S2} = r_{S3} = 23$ mΩ, $V_H = 42$ V, and $V_L = 14$ V.
3) Case 3: $r_{L1} = r_{L2} = 11$ mΩ, $r_{S1} = r_{S2} = r_{S3} = 23$ mΩ, $V_H = 42$ V, and $V_L = 10.5$ V.

Substituting these parameters into (56) and (67)–(69), the calculated efficiencies of the proposed and conventional converters in step-up and step-down modes are shown in Figs. 16

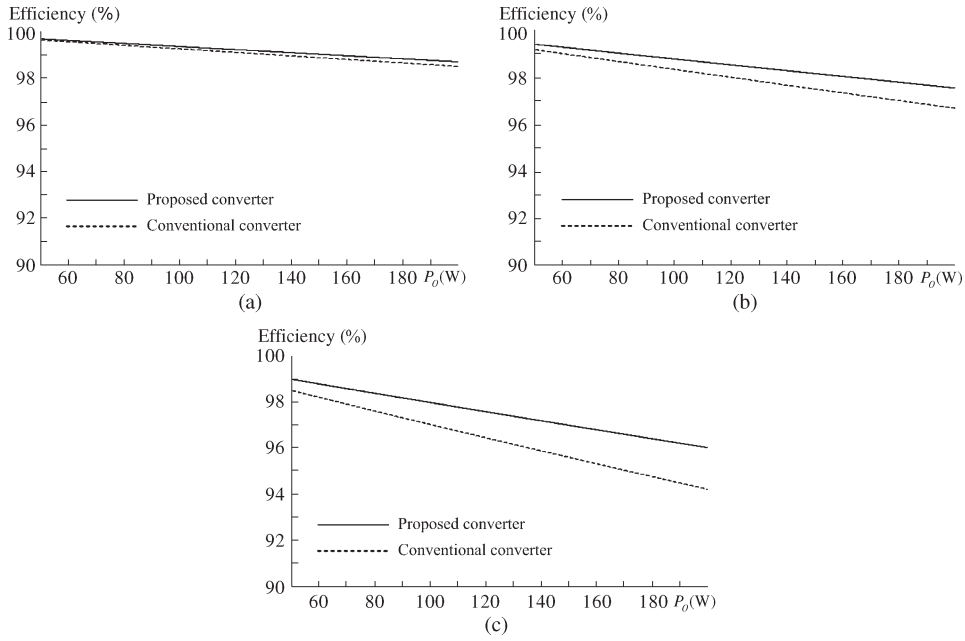

Fig. 16. Calculated efficiency of the proposed and conventional converters in step-up mode. (a) Case 1. (b) Case 2. (c) Case 3.

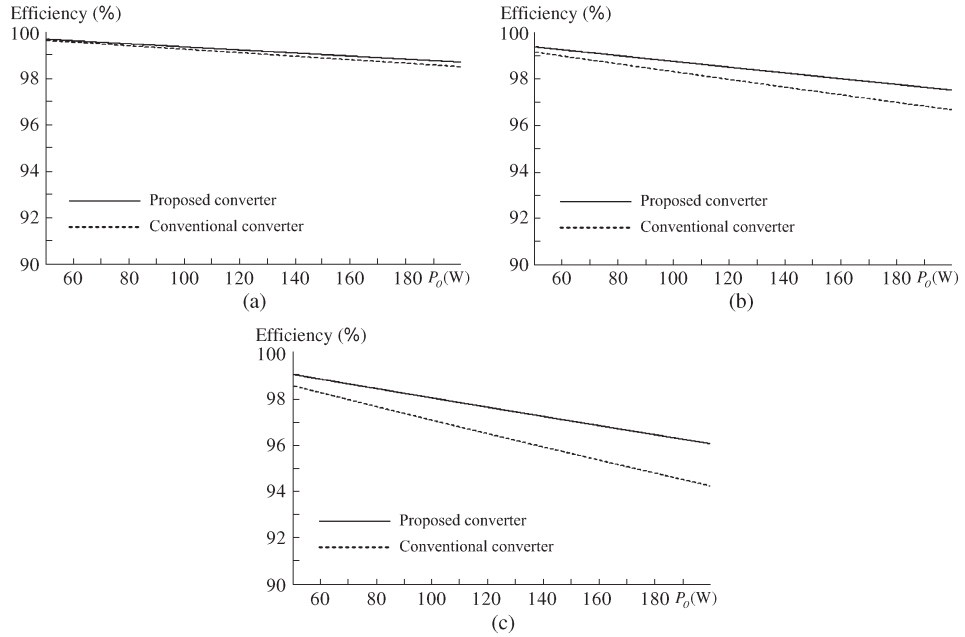

Fig. 17. Calculated efficiency of the proposed and conventional converters in step-down mode. (a) Case 1. (b) Case 2. (c) Case 3.

and 17, respectively. Thus, if the lower voltage gain is required, the conventional converter can be selected for lower cost. If the higher voltage gain is required, the proposed converter can be chosen for higher efficiency.

V. Experimental Results

In order to verify the performance of the proposed converter, a 14/42-V prototype circuit is built in the laboratory for the automobile dual-battery system. The electric specifications and circuit components are selected as $V_L = 14$ V, $V_H = 42$ V, $f_s = 50$ kHz, $P_o = 200$ W, $C_L = C_H = 330$ μF, $L_1 = L_2 = 15.5$ μH ($r_{L1} = r_{L2} = 11$ mΩ). Also, MOSFET IRF3710 ($V_{DSS} = 100$ V, $R_{DS(ON)} = 23$ mΩ, and $I_D = 57$ A) is selected for S_1, S_2, and S_3.

Some experimental results in step-up and step-down modes are shown in Figs. 18–21. Fig. 18(a) shows the waveforms of the input current i_L and the coupled inductor currents i_{L1} and i_{L2} in step-up mode. It can be seen that i_{L1} is equal to i_{L2}. The current i_L is double of the level of the coupled-inductor current during S_1/S_2 ON-period and equals the coupled-inductor current during S_1/S_2 OFF-period. Fig. 20(a) shows the waveforms of the current i_{LL} and the coupled-inductor currents i_{L1} and i_{L2} in step-down mode. It can be observed that i_{L1} is equal to i_{L2}. The current i_{LL} equals to the coupled-inductor current during S_3 ON-period and

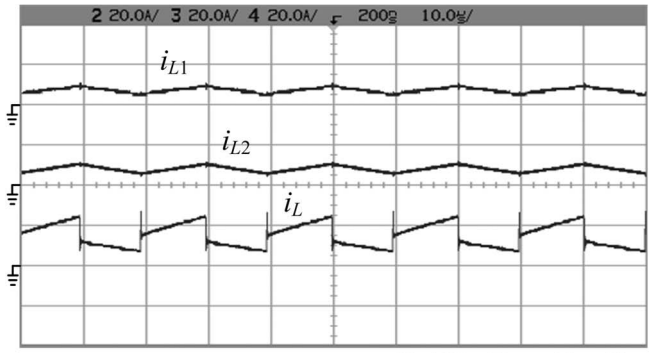

i_{L1}, i_{L2}, i_L: 20 A/div, Time: 10 μs/div

(a)

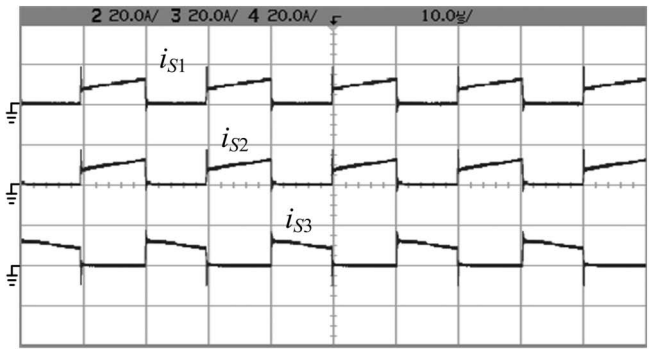

i_{S1}, i_{S2}, i_{S3}: 20 A/div, Time: 10 μs/div

(b)

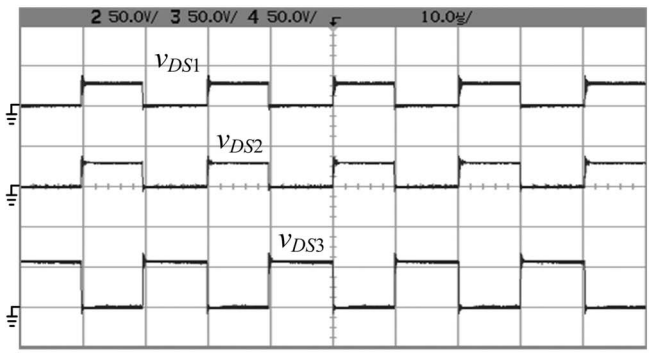

v_{DS1}, v_{DS2}, v_{DS3}: 50 V/div, Time: 10 μs/div

(c)

Fig. 18. Some experimental waveforms of the proposed converter in step-up mode. (a) i_{L1}, i_{L2}, and i_L, (b) i_{S1}, i_{S2}, and i_{S3}. (c) v_{DS1}, v_{DS2}, and v_{DS3}.

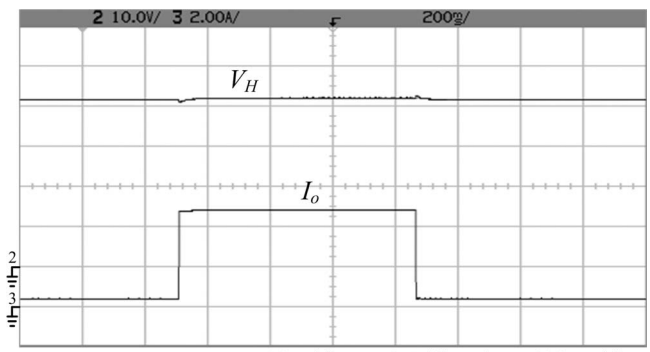

V_H: 10 V/div, I_o: 2 A/div, Time: 200 ms/div

Fig. 19. Dynamic response of the proposed converter in step-up mode for the output power variation between 20 and 200 W.

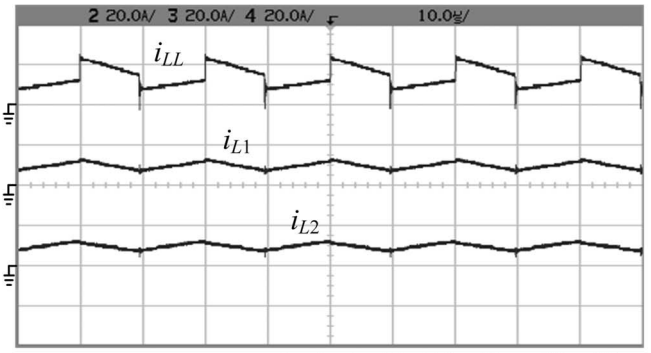

i_{LL}, i_{L1}, i_{L2}: 20 A/div, Time: 10 μs/div

(a)

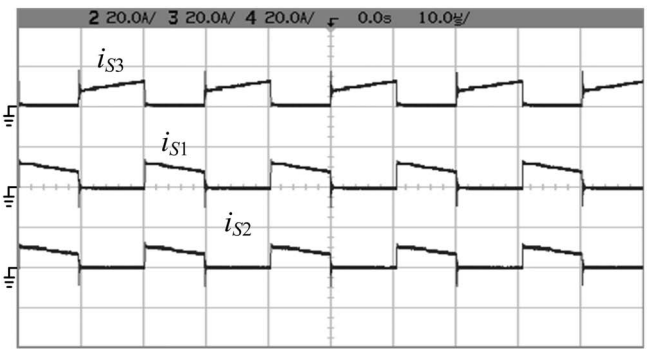

i_{S3}, i_{S1}, i_{S2}: 20 A/div, Time: 10 μs/div

(b)

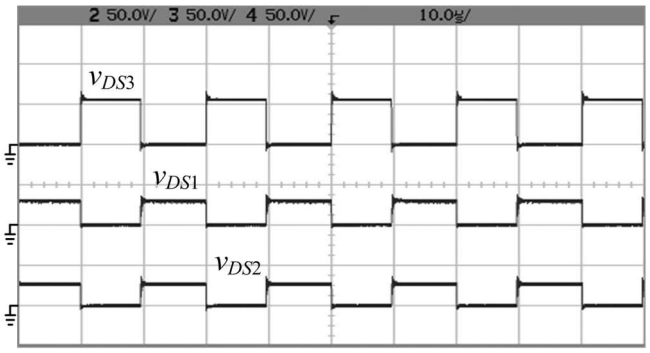

v_{DS3}, v_{DS1}, v_{DS2}: 50 V/div, Time: 10 μs/div

(c)

Fig. 20. Some experimental waveforms of the proposed converter in step-down mode. (a) i_{LL}, i_{L1}, and i_{L2}, (b) i_{S3}, i_{S1}, and i_{S2}. (c) v_{DS3}, v_{DS1}, and v_{DS2}.

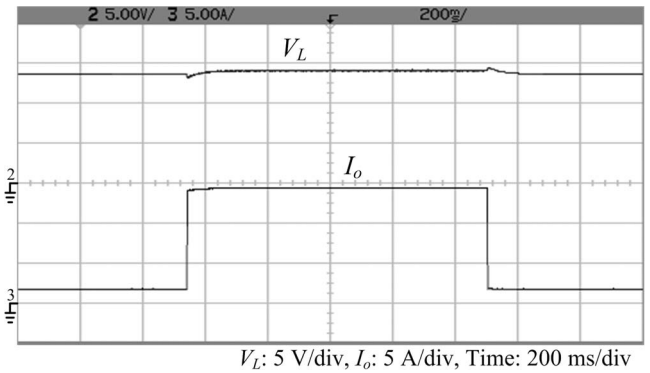

V_L: 5 V/div, I_o: 5 A/div, Time: 200 ms/div

Fig. 21. Dynamic response of the proposed converter in step-down mode for the output power variation between 20 and 200 W.

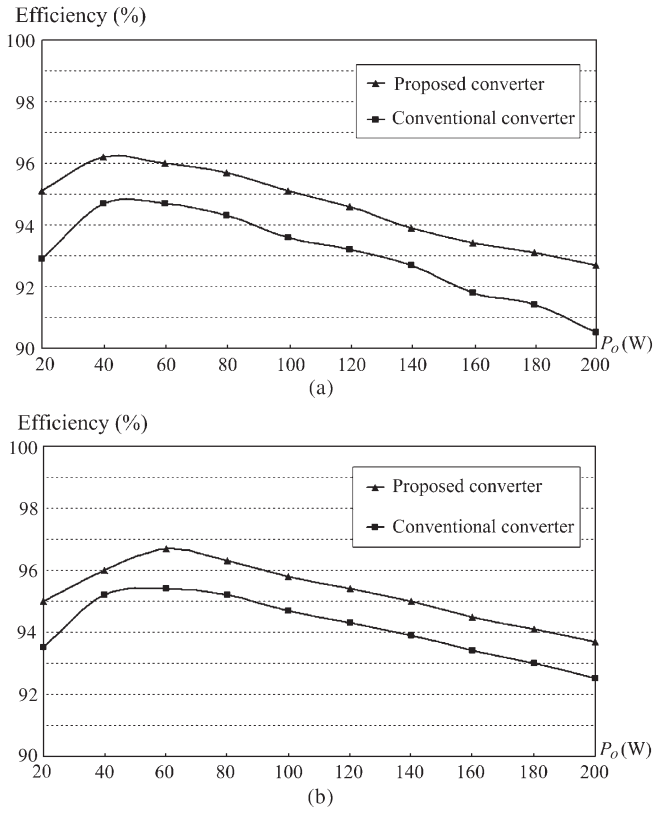

Fig. 22. Measured efficiency in the proposed converter and conventional bidirectional boost/buck converter. (a) Step-up mode. (b) Step-down mode.

is double of the level of the coupled-inductor current during S_3 OFF-period. Figs. 18(b) and 20(b) show the waveforms of the switch current i_{S1}, i_{S2}, and i_{S3} in step-up and step-down modes, respectively. As can be seen in Figs. 18(c) and 20(c), the voltage stresses on S_1 and S_2 equal $(V_H + V_L)/2$. Also, the voltage stress on S_3 equals $V_H + V_L$. Figs. 19 and 21 show the dynamic response of the proposed converter in step-up and step-down modes. One can see that the output voltage is well regulated.

Moreover, the prototype circuit of the conventional bidirectional boost/buck converter is also implemented in the laboratory. The electric specifications and circuit components are selected as $V_L = 14\,\text{V}$, $V_H = 42\,\text{V}$, $f_s = 50\,\text{kHz}$, $P_o = 200\,\text{W}$, $L_1 = 28\ \mu\text{H}$ $(r_{L1} = 15\ \text{m}\Omega)$, $C_L = C_H = 330\ \mu\text{F}$. Also, MOSFET IRF3710 is selected for S_1 and S_2. The measured efficiency in the proposed converter and the conventional bidirectional boost/buck converter are shown in Fig. 22. At full-load condition, the measured efficiency of the proposed converter is 92.7% in step-up mode and is 93.7% in step-down mode. Also, the measured efficiency of the proposed converter is around 92.7%–96.2% in step-up mode and is around 93.7%–96.7% in step-down mode. Also, it is seen from Fig. 22 that the measured efficiency of the proposed converter are higher than the conventional bidirectional boost/buck converter.

VI. Conclusion

This paper researches a novel bidirectional dc–dc converter. The circuit configuration of the proposed converter is very simple. The proposed converter has higher step-up and step-down voltage gains and lower average value of the switch current than the conventional bidirectional boost/buck converter. From the experimental results, it is see that the experimental waveforms agree with the operating principle and steady-state analysis. At full-load condition, the measured efficiency is 92.7% in step-up mode and is 93.7% in step-down mode. Also, the measured efficiency is around 92.7%–96.2% in step-up mode and is around 93.7%–96.7% in step-down mode, which are higher than the conventional bidirectional boost/buck converter.

References

[1] M. B. Camara, H. Gualous, F. Gustin, A. Berthon, and B. Dakyo, "DC/DC converter design for supercapacitor and battery power management in hybrid vehicle applications—Polynomial control strategy," *IEEE Trans. Ind. Electron.*, vol. 57, no. 2, pp. 587–597, Feb. 2010.

[2] T. Bhattacharya, V. S. Giri, K. Mathew, and L. Umanand, "Multiphase bidirectional flyback converter topology for hybrid electric vehicles," *IEEE Trans. Ind. Electron.*, vol. 56, no. 1, pp. 78–84, Jan. 2009.

[3] Z. Amjadi and S. S. Williamson, "A novel control technique for a switched-capacitor-converter-based hybrid electric vehicle energy storage system," *IEEE Trans. Ind. Electron.*, vol. 57, no. 3, pp. 926–934, Mar. 2010.

[4] F. Z. Peng, F. Zhang, and Z. Qian, "A magnetic-less dc–dc converter for dual-voltage automotive systems," *IEEE Trans. Ind. Appl.*, vol. 39, no. 2, pp. 511–518, Mar./Apr. 2003.

[5] A. Nasiri, Z. Nie, S. B. Bekiarov, and A. Emadi, "An on-line UPS system with power factor correction and electric isolation using BIFRED converter," *IEEE Trans. Ind. Electron.*, vol. 55, no. 2, pp. 722–730, Feb. 2008.

[6] L. Schuch, C. Rech, H. L. Hey, H. A. Grundling, H. Pinheiro, and J. R. Pinheiro, "Analysis and design of a new high-efficiency bidirectional integrated ZVT PWM converter for DC-bus and battery-bank interface," *IEEE Trans. Ind. Appl.*, vol. 42, no. 5, pp. 1321–1332, Sep./Oct. 2006.

[7] X. Zhu, X. Li, G. Shen, and D. Xu, "Design of the dynamic power compensation for PEMFC distributed power system," *IEEE Trans. Ind. Electron.*, vol. 57, no. 6, pp. 1935–1944, Jun. 2010.

[8] G. Ma, W. Qu, G. Yu, Y. Liu, N. Liang, and W. Li, "A zero-voltage-switching bidirectional dc–dc converter with state analysis and soft-switching-oriented design consideration," *IEEE Trans. Ind. Electron.*, vol. 56, no. 6, pp. 2174–2184, Jun. 2009.

[9] F. Z. Peng, H. Li, G. J. Su, and J. S. Lawler, "A new ZVS bidirectional dc–dc converter for fuel cell and battery application," *IEEE Trans. Power Electron.*, vol. 19, no. 1, pp. 54–65, Jan. 2004.

[10] K. Jin, M. Yang, X. Ruan, and M. Xu, "Three-level bidirectional converter for fuel-cell/battery hybrid power system," *IEEE Trans. Ind. Electron.*, vol. 57, no. 6, pp. 1976–1986, Jun. 2010.

[11] R. Gules, J. D. P. Pacheco, H. L. Hey, and J. Imhoff, "A maximum power point tracking system with parallel connection for PV stand-alone applications," *IEEE Trans. Ind. Electron.*, vol. 55, no. 7, pp. 2674–2683, Jul. 2008.

[12] Z. Liao and X. Ruan, "A novel power management control strategy for stand-alone photovoltaic power system," in *Proc. IEEE IPEMC*, 2009, pp. 445–449.

[13] S. Inoue and H. Akagi, "A bidirectional dc–dc converter for an energy storage system with galvanic isolation," *IEEE Trans. Power Electron.*, vol. 22, no. 6, pp. 2299–2306, Nov. 2007.

[14] L. R. Chen, N. Y. Chu, C. S. Wang, and R. H. Liang, "Design of a reflex-based bidirectional converter with the energy recovery function," *IEEE Trans. Ind. Electron.*, vol. 55, no. 8, pp. 3022–3029, Aug. 2008.

[15] S. Y. Lee, G. Pfaelzer, and J. D. Wyk, "Comparison of different designs of a 42-V/14-V dc/dc converter regarding losses and thermal aspects," *IEEE Trans. Ind. Appl.*, vol. 43, no. 2, pp. 520–530, Mar./Apr. 2007.

[16] K. Venkatesan, "Current mode controlled bidirectional flyback converter," in *Proc. IEEE Power Electron. Spec. Conf.*, 1989, pp. 835–842.

[17] T. Qian and B. Lehman, "Coupled input-series and output-parallel dual interleaved flyback converter for high input voltage application," *IEEE Trans. Power Electron.*, vol. 23, no. 1, pp. 88–95, Jan. 2008.

[18] G. Chen, Y. S. Lee, S. Y. R. Hui, D. Xu, and Y. Wang, "Actively clamped bidirectional flyback converter," *IEEE Trans. Ind. Electron.*, vol. 47, no. 4, pp. 770–779, Aug. 2000.

[19] F. Zhang and Y. Yan, "Novel forward-flyback hybrid bidirectional dc–dc converter," *IEEE Trans. Ind. Electron.*, vol. 56, no. 5, pp. 1578–1584, May 2009.

[20] H. Li, F. Z. Peng, and J. S. Lawler, "A natural ZVS medium-power bidirectional dc–dc converter with minimum number of devices," *IEEE Trans. Ind. Appl.*, vol. 39, no. 2, pp. 525–535, Mar. 2003.
[21] B. R. Lin, C. L. Huang, and Y. E. Lee, "Asymmetrical pulse-width modulation bidirectional dc–dc converter," *IET Power Electron.*, vol. 1, no. 3, pp. 336–347, Sep. 2008.
[22] Y. Xie, J. Sun, and J. S. Freudenberg, "Power flow characterization of a bidirectional galvanically isolated high-power dc/dc converter over a wide operating range," *IEEE Trans. Power Electron.*, vol. 25, no. 1, pp. 54–66, Jan. 2010.
[23] I. D. Kim, S. H. Paeng, J. W. Ahn, E. C. Nho, and J. S. Ko, "New bidirectional ZVS PWM sepic/zeta dc–dc converter," in *Proc. IEEE ISIE*, 2007, pp. 555–560.
[24] Y. S. Lee and Y. Y. Chiu, "Zero-current-switching switched-capacitor bidirectional dc–dc converter," *Proc. Inst. Elect. Eng.—Elect. Power Appl.*, vol. 152, no. 6, pp. 1525–1530, Nov. 2005.
[25] R. J. Wai and R. Y. Duan, "High-efficiency bidirectional converter for power sources with great voltage diversity," *IEEE Trans. Power Electron.*, vol. 22, no. 5, pp. 1986–1996, Sep. 2007.
[26] L. S. Yang, T. J. Liang, and J. F. Chen, "Transformerless dc–dc converters with high step-up voltage gain," *IEEE Trans. Ind. Electron.*, vol. 56, no. 8, pp. 3144–3152, Aug. 2009.

Lung-Sheng Yang was born in Tainan, Taiwan, in 1967. He received the B.S. degree in electrical engineering from National Taiwan Institute of Technology, Taipei, Taiwan, the M.S. degree in electrical engineering from National Tsing-Hua University, Hsinchu, Taiwan, and the Ph.D. degree in electrical engineering from National Cheng-Kung University, Tainan, in 1990, 1992, and 2007, respectively.

He is currently with the Department of Electrical Engineering, Far East University, Tainan, where he is an Assistant Professor. His research interests are power factor correction, dc–dc converters, renewable energy conversion, and electronic ballasts.

Tsorng-Juu Liang (M'93–SM'10) was born in Kaohsiung, Tainwan. He received the B.S. degree in electrophysics from National Chiao-Tung University, Hsinchu, Taiwan, in 1985, the M.S. and Ph.D. degrees in electrical engineering from the University of Missouri, Columbia, in 1990 and 1993, respectively.

From June 1987 to May 1989, he was employed as a Research and Design Engineer at TECO Electric and Machinery Company, Taiwan. From 1990 to 1993, he was a Research Assistant in the Power Electronics Research Center at the University of Missouri. From 1993 to 1998, he was an Assistant Professor in the department of Electrical Engineering at Kaohsiung Polytechnic Institute, Kaohsiung. Since 1998, he has worked with the department of Electrical Engineering at National Cheng-Kung University (NCKU), Tainan, where he is currently a Professor. Also, he was the Director of Electrical Laboratories at NCKU from 2001–2004. His research interests are inverter design, electronic ballast, dc–dc converters, switching power supply, back light inverter, renewable energy conversion, power integrated circuit, and high-power applications.

Dr. Liang is a member of the IEEE Power Electronics, Industrial Electronics, Circuits and Systems, and Industrial Applications Societies.